205-μm all-fiber laser source designed for CO 2 and wind coherent lidar measurement

Julien Lahyani, Julien Le Gouët, Fabien Gibert, Nicolas Cézard

2.05-µm all-fiber laser source designed for CO_2 and wind coherent lidar measurement

JULIEN LAHYANI[1], JULIEN LE GOUËT[1,*], FABIEN GIBERT[2] AND NICOLAS CEZARD[3]

[1]*DOTA, ONERA, Université Paris-Saclay, F-91123 Palaiseau, France*
[2]*Laboratoire de Météorologie Dynamique (LMD), Centre National de Recherche Scientifique (CNRS), Ecole Polytechnique, FR-91128 Palaiseau cedex, France*

[3]*ONERA/DOTA, Université de Toulouse, F-31055 Toulouse, France*
**julien.le_gouet@onera.fr*

Abstract: This work reports on an all-fiber pulsed laser source for simultaneous remote sensing of CO_2 concentration and wind velocity in the 2.05 µm region. The source is based on a polarization maintaining Master Oscillator Power Amplifier (MOPA) architecture. Two narrow-linewidth master oscillators for ON-line/OFF-line CO_2 DIAL operation alternately seed a four-stage amplifier chain at a fast switching rate up to 20 kHz. The MOPA architecture delivers laser pulses of 120 µJ energy, 200 ns duration (600 W peak power) at 20 kHz pulse repetition rate (2.4 W average power). The output linewidth is lower than 5 MHz, close to the pulse Fourier-Transform limit, and the beam quality factor is $M^2 = 1.12$. The source also provides a pre-amplified 20 mW local oscillator with a relative intensity noise of -160 dB/Hz that ensures optimal performance for future coherent detection.

1. Introduction

Carbon dioxide (CO_2) is widely acknowledged as the most important anthropogenic greenhouse gas in the atmosphere. Yet our understanding of its impact on future climate evolution still suffers some uncertainties [1]. To improve our knowledge of the CO_2 life cycle, and open ways to control anthropogenic emissions, it is necessary to quantify CO_2 fluxes around sources and sinks, at a local scale with ground-based instruments, and if possible, at the global scale with space-borne instruments.

Lidar sensors are especially attractive for such tasks, and several lidar systems based on high energy solid-state lasers already demonstrated good capabilities for CO_2 monitoring at 2 µm [2–5] and 1.5 µm [6–9], using DIfferential Absorption Lidar (DIAL) or Integrated Path Differential Absorption (IPDA). However, solid-state architectures generally involve large numbers of free-space optics that can raise substantial thermal and mechanical alignment issues when designing the observation system. All-fiber laser architectures alleviate those problems. In an assessment for a space-borne lidar (ASCENDS program), NASA Goddard Space Flight Center [8], based on a Fibertek heritage [10,11], and the Information Technology R&D Center of Mitsubishi Electric [12] both demonstrated for instance the interest of an all-fiber architecture in the 1.57 µm region. As a benchmark regarding pulse energy levels and repetition rates performed in previous works, solid-state cavities at 2.05 µm can reach tens of mJ at moderate repetition rate (usually lower than 1 kHz) [4], while all-fiber systems at 1.57 µm and 2.05 µm (including our system) reach hundreds of µJ at higher repetition rate (usually tens of kHz) [10]. Both technologies thus offer different trade-offs.

For space-borne monitoring with the IPDA technique, the 2.05 µm band is attractive, for it allows relaxing the requirement on the random error compared to1.57 µm. Indeed, the pressure dependence of the CO_2 R30 absorption line at 2051 nm offers a more favorable

Weighting Function (WF) in the low troposphere [13], where sources and sinks are localized [14]. Therefore, the development of a 2.05 µm all-fiber pulsed laser source, suitable for CO_2 monitoring, appears highly desirable in the perspective of future space-borne lidar system.

Fiber lidar systems also have the advantage to facilitate the use of coherent detection to perform range-resolved measurements of the wind speed. In the perspective of ground-based lidar systems, a fiber pulsed laser source at 2.05 µm could therefore offer a robust solution to measure simultaneously range-resolved profiles of the CO_2 Volume Mixing Ratio (VMR) and the wind speed, which is ideal for autonomous CO_2 flux rate measurements. Such dual function DIAL-Doppler lidars have already been reported for CO_2 [2,3] using solid-state lasers.

These systems could also find industrial interests. For example, the Physics Department of Montana state University [15] reported surface monitoring of CO_2 sequestration sites with a 1.57 µm fiber-based DIAL lidar, but they used direct detection and could not perform wind measurement simultaneously. Recently, our research group reported a fiber-based DIAL-Doppler lidar at 1.64 µm for industrial methane leaks monitoring, and demonstrated simultaneous CH_4/wind range-resolved profiles [16].

This study follows a bottom-up approach, with multiple potential applications that will not be discussed in details here. Of course, space requirements are very demanding and could not be fulfilled using the presented system. Ground-based industrial applications would generally require relaxed requirements, but with large variations depending of the scenario. Whatever the final application, building a powerful all-fiber laser source is a step forward, simpler and easier-to-deploy, for future lidar systems.

In this paper we report on the design and performance of a high peak-power, narrow-linewidth, all-fiber pulsed laser source at 2.05 µm, designed to be suitable for standalone km-range ground-based CO_2/wind measurement using coherent detection. To the best of our knowledge, this is the first all-fiber laser system at 2.05 µm that allows for such possibilities. In the first part, we describe and justify the objectives we had for the 2 µm fiber laser source, and remind relevant results of the literature in that field. In the second part, we describe the laser design. The last part is dedicated to experimental characteristics obtained with the laser source, in the perspective of upcoming DIAL-Doppler measurements.

2. Laser objectives

The CO_2 absorption line centered on 2050.97 nm (R30) has been identified in previous studies as one of the most promising for a space-borne lidar instrument [17]. According to the HITRAN database, the CO_2 R30 transition is about 4.3 GHz wide (at Full Width Half Maximum - FWHM) at 1 bar/293 °K in standard atmosphere, and is separated by 40 GHz from the nearest CO_2 absorption line. Therefore, the laser must offer narrow-linewidth in comparison to the absorption line width, and a tuning range of 20 GHz is desirable to allow full coverage of the R30 absorption line sideband. The ON and OFF wavelengths must also be close enough (typically < 1nm) to guarantee similar backscattering amplitude by the atmospheric aerosols or by hard-target surfaces.

To maximize the measurement accuracy and the lidar range, high laser pulse energy is necessary. Typically hundreds of µJ are required for range-resolved DIAL measurement with kilometer range in the boundary layer [2]. The pulse length should be between 100 ns and 1 µs, for the range-resolution to be between 15 and 150 m. The Pulse Repetition Rate (PRF) should be below 50 kHz to raise the ambiguity range up to 3 km. Fast wavelength switching is also required to ensure high atmospheric correlation between ON and OFF signals. For the

atmosphere to be considered as 'frozen', a switching rate of 1 kHz or more is typically required for ground-based systems [18]. In Table 1, we summarize the main laser features.

Table 1: Main laser features

Feature	Results in this study
Laser wavelength	2.05 µm
Spectral tunability	70 GHz (1 nm)
Pulse energy	120 µJ
Peak – Average power	600 W – 2.4 W
Pulse duration	200 ns
PRF	20 kHz
ON-OFF switch rate	Up to 20 kHz

Heterodyne measurement requires a Local Oscillator (LO) with low RIN (Relative Intensity Noise) in the analysis bandwidth. The fiber laser should exhibit a nearly Fourier-transform limited linewidth, a beam quality close to the diffraction limit (M^2=1) and a linear polarization. All these features play an important role on the Carrier-to-Noise Ratio (CNR) (see section 4). To minimize the bias made on the CO_2 VMR measurement, the spectral drift within the measurement time should be limited (or at least be monitored) to keep the bias as low as possible. High cross-talk isolation between ON-line and OFF-line beams and high Side-Mode Suppression Ratio (SMSR) are also required. In Table 2, we show the measured characteristics for all these parameters, with the associated error budgets in terms of CNR loss (random error) and CO_2 VMR bias budget (systematic error). These numbers are discussed in section 4.

Table 2: Laser-induced CNR loss/VMR bias budget

Features	Results in this study	CNR loss budget
RIN (around AOM frequency shift)	-160 dB/Hz	< 1 dB
Spectral Linewidth	<5 MHz	< 1 dB
Signal -LO beat frequency stability @ 10 ms	100 kHz	Negligible
Beam quality M^2	1,12	0.5 dB
Polarization, Polarization Extinction Ratio (PER)	Linear, PER > 16 dB	< 0.11 dB
		VMR bias budget
Frequency drift over 10 min	< 50 MHz (peak-to-peak)	<0.2%
Cross-Talk	-23 dB	<0.1% up to 3 km
SMSR	> 45dB	Negligible

Usually, power scaling of fiber-laser is limited by the extractible power or Stimulated Brillouin Scattering (SBS). As illustrated in [19], Tm-doped fiber amplifiers can deliver very high powers (up to 1 kW), and SBS can be partly circumvented by numerous methods [20]. In [21], a monolithic all-fiber amplifier delivering a high peak power of 10 kW for 100 ns pulses at 2.05 µm has also been demonstrated, but using a non-single-frequency seeder. We previously developed a 2.05 µm, single-frequency, 110 µJ, 110 ns, 20 kHz fiber laser source (2.2 W average power) [22]. However, this source was developed for optical parametric oscillator pumping, was mono-wavelength, and did not provide any LO output. Moreover,

this previous source unfortunately exhibited high RIN and also suffered power instabilities. The following sections explain how the source has been re-designed, upgraded, and fully characterized to comply with our objectives for combined lidar measurement of CO_2 and wind.

3. Experimental setup

The amplification chain is shown on Fig 1 and is detailed in following subsections. The source architecture is based on a Polarization Maintaining (PM) Master Oscillator Power Fiber Amplifier (MOPFA) made of four Thulium Doped Fiber Amplifiers (TDFA) pumped at 793 nm. The MOPFA is seeded alternatively by two narrow-linewidth Distributed Feed-Back Laser Diodes (DFB-LD) using an Optical Switch (OS). The pre-amplifier (TDFA1, detailed in section 3.1) delivers a continuous signal. The optical power at its output is split in two parts, one delivering the LO power and one seeding the second amplifier. An AOM (Acousto-Optic Modulator) shapes the signal into pulses and adds an optical frequency offset for heterodyne detection. The TDFA2 and the pulse shaping system are described in section 3.2. At its output, a Mach-Zehnder Electro Optic Modulator (EOM) is used as a time-gated attenuator to filter amplified AOM parasitic spikes. Since the last two amplifiers, (including ASE filtering, Stimulated Brillouin Scattering (SBS) monitoring, and fiber strain gradient for SBS gain reduction) are identical to those reported in [22], only general features of TDFA3 and TDFA4 are reminded in section 3.3. Finally, the output of TDFA4 is spliced to a simple-clad LMA fiber that is crimped into a FC-APC connector, allowing for an easy coupling to the lidar emission optics.

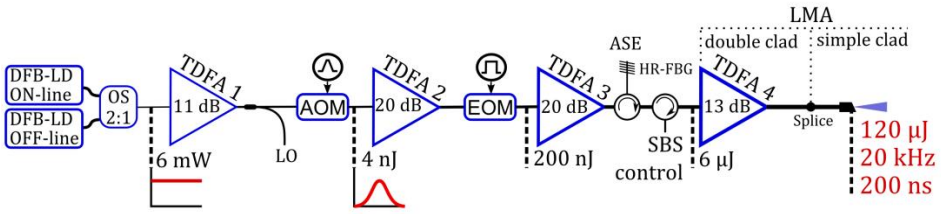

Fig 1: Schematic of the MOPFA. Energy values are given for 200 ns pulses at 20 kHz repetition rate. DFB-LD: Distributed Feedback Laser Diode, OS: Optical Switch, LO: Local Oscillator, TDFA: Thulium Doped Fiber Amplifier, AOM: Acousto-Optic Modulator, EOM: Electro-Optic Modulator, ASE: Amplified Spontaneous Emission, HR-FBG: High Reflectivity Fiber Bragg Grating, SBS: Stimulated Brillouin Scattering, LMA: Large Mode Area.

3.1 Continuous wave pre-amplification for LO derivation

In many coherent fiber lidar designs, a fraction of the CW (Continuous Wave) laser seed is directly derived to be used as LO, and the rest is shaped before amplification [23]. In our case, a LO power of 20 mW (able to provide 1 mW power at the detector after a 95:5 coupler) is necessary for the heterodyne measurement. However, the power delivered by the DFB-LD is limited to 10 mW, and the optical switch introduces losses. Moreover, DIAL measurement may also require a wavelength calibration or monitoring channel that would require another fraction of the DFB-LD CW power. Therefore, it was necessary to pre-amplify the signal, without degrading the intensity noise. The seeders, OS and CW pre-amplifier are illustrated in Fig 2.

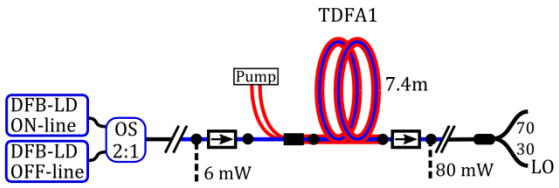

Fig 2. Schematic of the DFB-LD with the OS seeding the pre-amplifier (TDFA1). The two boxes with right-directed arrows are optical isolators

The OS is an electro-optic-based system (Agiltron Inc – NSSW-120110333). It permits a switching repetition rate up to 100 kHz with rise and fall times lower than 300 ns. As the laser PRF requirement must be under 50 kHz, it allows for pulse-to-pulse switching if necessary. In the configuration presented here the PRF is 20 kHz. However the OS exhibits some cross-talk between the input channels. This issue and its expected impact on the lidar performance is discussed later in section 4.5.

The TDFA1 provides up to 80 mW with 3% RMS stability over 10 minutes. The isolators prevent backscattered light from disturbing the DFB-LD operation, especially its spectral linewidth and RIN. The pump power is delivered by two LD at 793 nm. The pump beam is co-propagative with the signal into the 7.4 m Tm-doped fiber length. The latter is longer than the 4 m length that would maximize the signal power, but it generates a weaker ASE fraction (0.07% of total power). The LO derivation is provided by a 70:30 coupler where the 30% LO arm delivers about 20 mW.

Compared to the pre-amplifier previously reported in [22], this new pre-amplifier has lower power (80 mW instead of 1 W) but it exhibits much lower RIN and thermal fluctuations. In the former pre-amplifier, the power could fluctuate by up to 50% peak-to-peak during the first minutes after turning on. These variations make it difficult to control the LO power and could damage the detector. They stemmed probably from temperature fluctuations caused by the high optical intensity, that could favor fluctuations of non-radiative relaxations [24]. Moreover, the RIN in the AOM frequency shift analysis bandwidth was -150 dB/Hz. This was 20 dB higher than the value at the DFB-LD output, and was due to the beat note between the LO and the high ASE power near the signal wavelength. Consequently, this new pre-amplifier is much more suitable and reliable for deriving a high-quality LO signal, while remaining powerful enough to feed the subsequent amplification stages in a convenient power regime.

3.2 Pulse shaping and pre-amplification

An AOM is placed before TDFA2 to perform simultaneously the pulse shaping and the 80 MHz frequency shift. The pulse duration is set to 200 ns, corresponding to 30 m lidar resolution. The laser PRF is set to 20 kHz, which ensures a lidar ambiguity distance of 7.5 km, sufficient for ground-based measurements. A high PRF is also interesting to average a large number of shots and reduce the atmospheric speckle noise for coherent detection [25].

The electronic command for the AOM driver is a trapezoidal pulse with a slower leading edge to pre-compensate the gain alteration during the pulse amplification [26]. Thanks to the AOM rise and fall times, the resulting optical pulses exhibit a bell-shape temporal profile (Fig 3 (a)). While testing our lidar coherent detection, we found that the CNR was degraded by a residual bounce of the AOM-transmitted light, about 4 µs after trigger time. This parasitic pulse is caused by reflections of the acoustic wave in the AOM crystal. Its amplitude was about 48 dB lower than the main pulse (typical AOM characteristic). In our tests, this level proved to be high enough to strongly disturb the lidar signal at 600 m of distance (corresponding to 4 µs in delay). We thus inserted a Mach-Zehnder Electro Optic Modulator

(EOM) at the TDFA2 output to add 20 dB of extinction between pulses. At this position the EOM also filters about 9 dB of the ASE power produced by the TDFA2 between pulses. The EOM electronic command is a square pulse centered on the optical pulse and 3 times longer. Eventually, the TDFA2 provides optical pulses of 200 nJ to the third amplifier (TDFA3), with an ASE fraction lower than 2%.

3.3 Power amplification

The power amplification gain is distributed over two stages (TDFA3 and TDFA4) in order to limit the fiber warming. Compared to [22], the TDFA3 is seeded with a higher peak power. Therefore, a lower pump power is required to reach the same output power, thus limiting the thermal heating and signal power fluctuations. The high reflectivity FBG is centered at 2051.2 m, with a 1 nm width. The limitation of the output power by Brillouin scattering is alleviated by introducing a strain gradient along the fiber. The gradient profile is chosen to avoid strain discontinuities that would alter the fiber lifetime. The SBS threshold peak power has been measured to 800 W at the TDFA4 output, but in order to prevent laser pump warming over long time measurement, a working point of 120 µJ/pulse, 200 ns, 20 kHz was finally chosen (600 W peak power). The characterization of the full laser source is detailed below for this working point.

4. Laser performance for DIAL-Doppler applications

The following section is dedicated to the experimental evaluation of the laser source parameters presented in section 2 (and Table 2) for DIAL-Doppler applications.

4.1 Laser-induced noise sources

The quality of coherent lidar signals is often expressed through the Carrier-to-Noise Ratio (CNR), defined by:

$$CNR(\mathrm{z}) = \frac{\left\langle i_{het}^2 \right\rangle}{\left\langle i_{noise}^2 \right\rangle} \tag{1}$$

The angle brackets denote the mean value, i^2_{het} is the heterodyne current power and i^2_{noise} the noise current power. In [27], the noise power in presence of a pre-amplifier is detailed. The CNR expression can thus be developed to highlight the most important features as followed:

$$CNR(\mathrm{z}) = \frac{2.P_S.P_{LO}.S^2.\Gamma(z,\lambda).z^{-2}}{\left(\sigma_{shot}^2 + \sigma_{RIN}^2 + \sigma_{\mathrm{det}}^2\right).B_e} \tag{2}$$

where :

$\sigma_{shot}^2 = 2.e.S.P_{LO}$,

$\sigma_{RIN}^2 = (RIN_{seed} + RIN_{LO-ASE}).S^2.\mathrm{P}_{LO}^2$,

$RIN_{LO-ASE} = 4.\xi.B_o^{-1}.r$,

$\sigma_{\mathrm{det}}^2 = S^2.NEP^2$.

Table 3. Parameters used for theoretical calculation of CNR

Parameters	Meaning and unit	Parameters	Meaning and unit
Ps	Received signal power (W)	**Be**	Electronic integration bandwidth (Hz)
P_{LO}	LO optical power (W)	***e***	Elementary charge (C)
S	Detector sensitivity (A/W)	**RIN_{seed}**	Seeder relative intensity noise (dB/Hz)
Γ	Lidar and atmospheric parameters (m^2)	**RIN_{LO-ASE}**	LO-ASE beat note relative intensity noise (dB/Hz)
z	Distance of propagation (m)	**ξ**	ASE fraction in LO
σ_{shot}	Shot noise ($A/Hz^{1/2}$)	**B_O**	Optical bandwidth of the ASE (Hz)
σ_{RIN}	Relative intensity noise ($A/Hz^{1/2}$)	***r***	Ratio between the ASE spectral power near the LO wavelength and at its emission peak
σ_{det}	Electronic noise ($A/Hz^{1/2}$)	**NEP**	Noise Equivalent Power of the detector ($W/Hz^{1/2}$)

All the parameters of Eq.(2) are summarized in Table 3. The optimal sensitivity for heterodyne detection is achieved when the noise current is dominated by the shot noise (quantum limit).

The impact on the CNR induced by the measured figures of RIN_{seed} and RIN_{LO-ASE} are calculated in Table 2, assuming a detector sensitivity S of 1.2 A/W, a NEP of 8 $pW/Hz^{1/2}$ (measured value of our detector around 80 MHz) and a P_{LO} of 800 µW. The RIN of the DFB-LD (RIN_{seed}) is lower than -170 dB/Hz around 80 MHz, and therefore it represents a negligible contribution to the noise power. The RIN induced by the LO-ASE beat note (RIN_{LO-ASE}) is -160 dB/Hz which is consistent with the measured ASE fraction in the LO, B_o and r which are respectively 0.07%, 4.9 THz (i.e. 65 nm) and 0.2. Then, the degradation of the CNR due to the RIN of the LO is lower than 1 dB. As a comparison, a RIN of -150 dB/Hz would degrade the CNR by 5 dB.

4.2 Spectral linewidth

As mentioned in section 2, the beat note spectrum of the heterodyne signal must be as narrow as possible. Its linewidth is determined by the LO linewidth, the pulse profile, and the pulse-to-pulse beat note frequency jitter in case of time averaging. Therefore, we wanted to verify whether the pulse spectrum and time profile were close to the Fourier-transform (FT) limit, and if the beat note frequency was sufficiently stable over time.

The beat note between the output laser signal and the LO is obtained by mixing a small fraction of the emitted pulses with the LO through a fiber coupler. The signal is then detected with a fast photodiode at 250 MHz sampling rate (Fig 3 (b)). The LO is delayed by 39 m in order to compensate the optical path difference induced by the fiber length of the complete amplifier. This permits the analysis of the spectral broadening due to the pulse shaping and potential chirp induced by amplification, while cancelling the DFB-LD phase noise contribution. The beat note signal Power Spectral Density (PSD) is calculated using a discrete FT of the auto-correlation function, and averaged over 200 shots (Fig 3 (c)). For the measurement of the Time-Bandwidth Product (TBP), we also monitored the pulse shape (Fig 3 (a)).

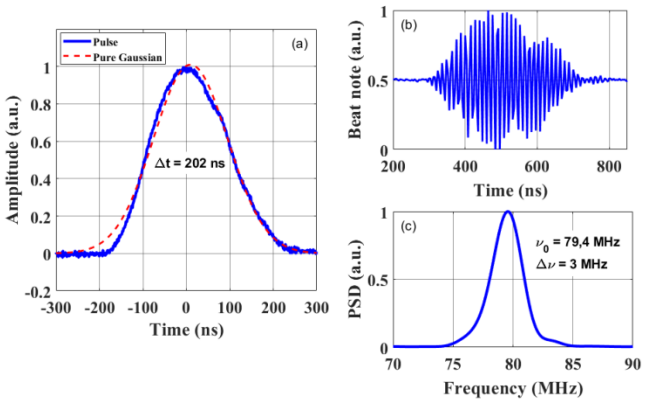

Fig 3. (a) Pulse shape at the TDFA4 output (blue) and Gaussian fit (red, dashed). (b) Beat note between the LO and the emitted pulse and (c) the PSD averaged over 200 shots. Δt: pulse duration at FWHM, Δν: spectral linewidth at FWHM, ν_0: beat note center frequency

The average spectral broadening caused by pulse shaping and amplification is 3 MHz at FWHM. The TBP is 0.6, whereas the FT limit is 0.44 for Gaussian pulses. For a lidar configuration, where the LO and signal path differences cannot be balanced, the total spectral linewidth is the convolution of the DFB-LD PSD (induced by phase noise with Lorentzian profile) and the spectral broadening mentioned before. For instance, the linewidth of the convolution between a Lorentzian shape (2 MHz) and a Gaussian shape (3 MHz) is 4.2 MHz. We measured the total spectral linewidth using a delay line of 1 km (fully decorrelated interferometer) and found it to be lower than 5 MHz, which agrees with the DFB-LD linewidth (~2 MHz).

The gain variations during pulse amplification induce a slight frequency chirp, so that the beat note frequency is shifted by 0.5 to 1 MHz from the 80 MHz AOM shift. The resulting bias on the wind velocity measurement is 0.5 to 1 m/s. This bias can be corrected using a beat note reference (e.g. generated by the backscattering signal from the lidar emission optics).

To determine some potential spectral broadening due to frequency jitter when averaging lidar shots, we calculated the Allan deviation of the beat note frequency with a 1 km delay line between the LO and signal.

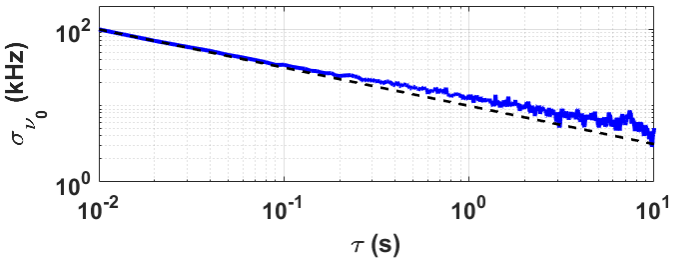

Fig 4. Allan standard deviation (blue) of the beat note frequency calculated from a dataset of 5 minutes (plotted over 10 s to minimize the statistical error) and -1/2 slope (black, dashed) representing the stationary behavior. LO and signal are delayed by 1 km. σ: Allan standard deviation, ν_0: beat note frequency

The Allan standard deviation of the beat note frequency is shown on Fig 4. At 10 ms averaging time (i.e. 200 shots) the standard deviation is 100 kHz (2% of spectral linewidth). At 100 ms averaging time, it decreases to 30 kHz (lower than 1% of spectral linewidth). The linewidth of the averaged PSD function is defined by the convolution of the spectral linewidth

of the laser with the beat note frequency dispersion. Thus, averaging shots over 10 ms to 10 s (maximum averaging time of this measurement) will not degrade the CNR

4.3 Beam quality and polarization

At the final fiber output, the laser beam is collimated by an aspheric lens that does not alter the M^2 factor. The measurement is made by fitting the beam diameter (D4σ definition) along the propagation axis (Fig 5). A least square fit provides an estimation of the waist at the focal plane and of the divergence that defines the M^2.

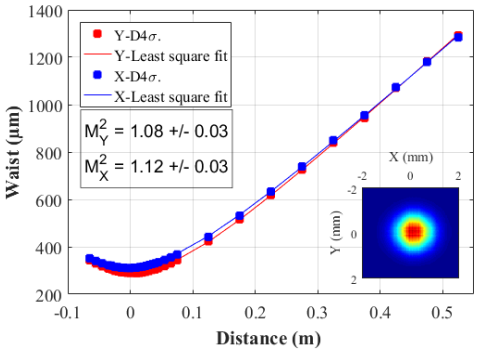

Fig 5. M^2 estimation of laser beam at 120 µJ in two perpendicular directions. Laser beam is focused by a 2", f = 400 mm lens

The beam quality factor is estimated to M^2 = 1.08 for Y-direction and M^2 = 1.12 for X-direction. The CNR dependence to M^2 is expressed in [23], which indicates that a M^2 of 1.12 induces 0.5 dB loss on the CNR compared to a diffraction limited beam (M^2=1).

The Polarization Extinction Ratio (PER) has also been measured and is higher than 16 dB. As the interference between the LO and the lidar signal requires the same polarization state, the higher is the PER, the higher is the heterodyne efficiency. The relative degradation of the CNR induced by the PER is expressed as:

$$\frac{CNR(\mathrm{PER})}{CNR(\infty)} = 1 - \frac{1}{PER} \qquad (3)$$

In our case, the PER degrades the CNR by less than 0.11 dB compared to a perfectly linearly polarized beam.

4.4 Frequency tuning and stability

The laser spectral tuning range is shown on Fig 6, together with the absorption lines of CO_2 and H_2O. In our case, the laser source tuning range is limited by the FBG spectral width of 1 nm (70 GHz). Our DFB-LD is tunable over this range using the temperature setting. As mentioned in section 2, this is sufficient to probe the R30 absorption line. In future works, a slight shift of the FBG spectrum would be an interesting upgrade to also permit H_2O VMR measurement using the 2050.5 µm H_2O absorption line. Such a multispecies DIAL-Doppler lidar would then be able to monitor simultaneously two major greenhouse gases [28].

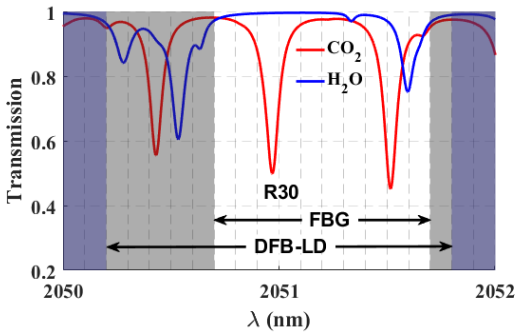

Fig 6. CO_2 (red) and H_2O (blue) horizontal transmission for 2 km propagation through standard atmosphere. The white background represents the total laser spectral tuning.

The absolute spectral stability is also an important parameter for the accuracy of DIAL measurement, as any uncontrolled variation of the ON-line frequency would directly reflect on the cross-section difference (see Eq.(4) below). To infer the absolute frequency of the laser, we measured the transmission through a gas cell filled with pure CO_2. The laser wavelength is set on the R30 sideband to maximize the sensitivity. We find a peak-to-peak drift lower than 50 MHz over ten minutes (standard deviation of 20 MHz). This error would convert into a 0.2% bias on a CO_2 VMR measurement, in the case of an ON-line wavelength set on the center of the R30 absorption line. Some studies have demonstrated that DFB-LD frequency stabilization schemes can achieve frequency stabilities better than 1 MHz over hours [29,30]. For preliminary lidar measurements, implementing such a frequency-stabilizing sub-system is not a priority, but it will be integrated to our emitter in future works.

4.5 Spectral purity impact on DIAL measurement

The OS presents a residual cross-talk, which is a fraction of the switched-off arm transmitted to the output. Fig 7 represents the optical spectrum at the OS output for the two switch positions. We define position 1 as the transmission of the OFF-line DFB-LD and extinction of the ON-line, and position 2 as the opposite. The cross-talk is -23 dB for both positions. We measured the same values at the TDFA4 output, indicating that the amplification chain does not degrade the cross-talk. We found however that the cross-talk value is sensitive to temperature fluctuations. Significant cross-talk variations (~ 5dB) have been measured on each arm, which could have been an issue for DIAL measurements. Therefore, we used a supplementary Peltier module to manage the OS temperature and maintain stable cross-talk isolation over time.

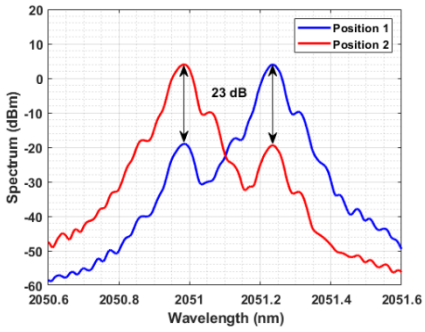

Fig 7. Optical spectrum of the DFB-LD at the OS output.

The cross-talk impact on the expected lidar CNR can be derived from the following rationale. From the classical DIAL equation described in [31], the CO_2 VMR estimation, biased by the residual signal at the switched-off wavelength, writes:

$$\rho_{CO_2} + \rho_{bias} = \frac{1}{\Delta x_{\sec}} . \frac{d}{dz} \left(\frac{1}{2} . \ln \left[\frac{CNR_{OFF}(1+\varepsilon_{OFF})}{CNR_{ON}(1+\varepsilon_{ON})} \right] \right) \quad (4)$$

where ρ_{CO2} is the gas VMR, ρ_{bias} the systematic error due to the cross-talk, Δx_{sec} the CO_2 cross-section difference at ON/OFF-line wavelengths, $CNR_{OFF/ON}$ the carrier to noise ratio of the OFF-line signal and the ON-line signal respectively and ε the relative error on the CNR due to the cross-talk. By identification, we can write:

$$\rho_{bias} = \frac{1}{\Delta x_{\sec}} . \frac{d}{dz} \left[\frac{1}{2} . \ln \left(\frac{1+\varepsilon_{OFF}}{1+\varepsilon_{ON}} \right) \right] \quad (5)$$

To evaluate ε, we modify the usual CNR (see Eq.(1)) by adding $\langle i^2_\chi \rangle$, the heterodyne signal due to the cross-talk, and assuming that the cross-talk induces negligible noise:

$$CNR(\mathrm{z}) = \frac{\left\langle i^2_{het} \right\rangle + \left\langle i^2_\chi \right\rangle}{\left\langle i^2_{noise} \right\rangle} \quad (6)$$

For a cross-talk fraction χ the undesired optical power is $P_\chi = \chi.P$. As the cross-talk is conserved along the amplification, we can write from Eq.(2):

$$\left\langle i^2_\chi \right\rangle = 2.\chi^2 . P_{LO} . P_S . S^2 . \Gamma(\mathrm{z}, \lambda_\chi) . \mathrm{z}^{-2} \quad (7)$$

where λ_χ is the switched-off wavelength. We can then express ε as:

$$\varepsilon = \frac{\left\langle i^2_\chi \right\rangle}{\left\langle i^2_{het} \right\rangle} = \chi^2 . \frac{T_{atm}(\mathrm{z}, \lambda_\chi)}{T_{atm}(\mathrm{z}, \lambda)} \quad (8)$$

where T_{atm} is the atmospheric transmission. From Eq.(7,8) we calculate that a cross-talk χ=-23 dB on both the LO and laser output beams causes a relative bias lower than 0.1% on the CO_2 measurement over 3 km of propagation.

The presence of side-modes in the DFB-LD spectrum can also induce a bias on the CO_2 VMR measurement. We can extend the calculation presented before to compute the impact of these side-modes, by modifying Eq.(7):

$$\left\langle i^2_{SM} \right\rangle = 2.n_{SM} . SMSR^{-2} . P_{LO} . P_S . S^2 . \Gamma(\mathrm{z}, \lambda_{SM}) . z^{-2} \quad (9)$$

where n_{SM} is the number of side modes, SMSR the Side-Mode Suppression Ratio and λ_{SM} the wavelengths of side-modes. The SMSR of our DFB-LD is over 45 dB, and 56 dB at the

TDFA4 output. We measured about 250 side modes in our DBF-LD. The relative bias on the CO_2 VMR will thus be less than 0.03%.

Due to the presence of two distinct wavelengths in the amplifiers, Four-Waves Mixing (FWM) occurs and produces additional sidebands. These sidebands are not visible in the LO (TDFA1 output), probably due to low intensity. However, it is visible in the last amplifier where the intensity is three orders of magnitude higher. As the LO is clear of additional sidebands, FWM does not bring any additional interferences with the emitted pulse that could fall in the detector band-pass. It has therefore no measurable impact on the VMR bias.

5. Conclusion

In this work, we demonstrated a 2.05µm all-fiber laser source that meets the requirements of a DIAL-Doppler emitter for remote sensing of atmospheric CO_2 and wind. The architecture allows a spectral tunability of 70 GHz around the R30 CO_2 absorption line, a LO RIN of -160 dB/Hz, a spectral linewidth lower than 5 MHz (close to the Fourier limit) with a Signal-LO beat note frequency short term stability of 100 kHz at 10 ms, a frequency drift lower than 50 MHz peak-to-peak over 10 min (free-running operation), a crosstalk of -23 dB between ON-line and OFF-line wavelengths and a LO SMSR higher than 45 dB and higher than 56 dB in the final stage. The laser exhibits a beam quality factor of M^2=1.12 and a PER higher than 16 dB. The addition of all the noise contributions listed above reduces the CNR by less than 2.6 dB. The main contributions are the RIN of the pre-amplified LO and the spectral profile. At the moment the CO_2 VMR measurement could be biased by 0.3% due to cross-talk and potential spectral drifts of the (currently) free-running seeder. Implementing a spectral stabilization sub-system would overcome this last drawback.

The demonstrated laser source reaches an average power of 2.4 W (at 20 kHz rate) and high pulse peak power of 600 W (120 µJ, 200 ns). Yet it is known that non-linear effects (especially SBS) can limit the peak power in fiber laser systems to a much lower value than in solid-state laser cavities. A future step of this work is therefore to inject the fiber output beam into a solid-state amplifier for peak-power upscaling. A single-pass solid-state amplification is under assessment, which would minimize alignment issues. The resulting hybrid fiber/solid-state laser source could represent an attractive trade-off combining high peak-power and limited free-space optics complexity, as required for long-range systems and future space-borne lidar missions.

Funding

ONERA & CNES co-funding agreement (ONERA 9709 / CNES 5100018351)

Acknowledgement

The authors are especially thankful to Benoit Faure (CNES) for supporting this project. We also wanted to thank Didier Goular and Christophe Planchat for their important technical support.

Disclosures

The authors declare no conflicts of interest.

References

1. R. K. Pachauri, L. Mayer, and Intergovernmental Panel on Climate Change, eds., *Climate Change 2014: Synthesis Report* (Intergovernmental Panel on Climate Change, 2015).
2. F. Gibert, P. H. Flamant, D. Bruneau, and C. Loth, "Two-micrometer heterodyne differential absorption lidar measurements of the atmospheric CO2 mixing ratio in the boundary layer," Appl. Opt., AO **45**, 4448–4458 (2006).

3. S. Ishii, K. Mizutani, H. Fukuoka, T. Ishikawa, B. Philippe, H. Iwai, T. Aoki, T. Itabe, A. Sato, and K. Asai, "Coherent 2 μm differential absorption and wind lidar with conductively cooled laser and two-axis scanning device," Appl. Opt., AO **49**, 1809–1817 (2010).
4. U. N. Singh, B. M. Walsh, J. Yu, M. Petros, M. J. Kavaya, T. F. Refaat, and N. P. Barnes, "Twenty years of Tm:Ho:YLF and LuLiF laser development for global wind and carbon dioxide active remote sensing," Opt. Mater. Express, OME **5**, 827–837 (2015).
5. E. Cadiou, D. Mammez, J.-B. Dherbecourt, G. Gorju, J. Pelon, J.-M. Melkonian, A. Godard, and M. Raybaut, "Atmospheric boundary layer CO2 remote sensing with a direct detection LIDAR instrument based on a widely tunable optical parametric source," Opt. Lett., OL **42**, 4044–4047 (2017).
6. A. Amediek, A. Fix, M. Wirth, and G. Ehret, "Development of an OPO system at 1.57 μm for integrated path DIAL measurement of atmospheric carbon dioxide," Appl. Phys. B **92**, 295–302 (2008).
7. D. Sakaizawa, S. Kawakami, M. Nakajima, Y. Sawa, and H. Matsueda, "Ground-based demonstration of a CO2 remote sensor using a 1.57μm differential laser absorption spectrometer with direct detection," JARS **4**, 043548 (2010).
8. A. W. Yu, J. B. Abshire, M. Storm, and A. Betin, "Laser amplifier development for IPDA Lidar measurements of CO 2 from space," in *Proc. SPIE* (2015), Vol. 9342.
9. A. Amediek, G. Ehret, A. Fix, M. Wirth, C. Büdenbender, M. Quatrevalet, C. Kiemle, and C. Gerbig, "CHARM-F—a new airborne integrated-path differential-absorption lidar for carbon dioxide and methane observations: measurement performance and quantification of strong point source emission," Appl. Opt., AO **56**, 5182–5197 (2017).
10. W. Lu, D. Engin, M. Storm, and S. Gupta, "High-power narrow linewidth 1.5-um fiber-amplifier lidar transmitter for atmospheric CO2 detection," in *Fiber Lasers XI: Technology, Systems, and Applications* (International Society for Optics and Photonics, 2014), Vol. 8961, p. 89610C.
11. S. Gupta, D. Engin, K. Puffenberger, S. Litvinovich, F. Kimpel, and R. Utano, "Fiber laser systems for space lasercom and remote sensing," in E. W. Taylor and D. A. Cardimona, eds. (2013), p. 88760E.
12. S. Kameyama, M. Imaki, Y. Hirano, S. Ueno, S. Kawakami, D. Sakaizawa, and M. Nakajima, "Development of 1.6 μm continuous-wave modulation hard-target differential absorption lidar system for CO2 sensing," Opt. Lett., OL **34**, 1513–1515 (2009).
13. R. T. Menzies and D. M. Tratt, "Differential Laser absorption spectrometry for global profiling of tropospheric carbon dioxide: selection of optimum sounding frequencies for high-precision measurements," Appl. Opt., AO **42**, 6569–6577 (2003).
14. P. J. Rayner and D. M. O'Brien, "The utility of remotely sensed CO2 concentration data in surface source inversions," Geophysical Research Letters **28**, 175–178 (2001).
15. W. Johnson, K. S. Repasky, and J. L. Carlsten, "Micropulse differential absorption lidar for identification of carbon sequestration site leakage," Appl. Opt., AO **52**, 2994–3003 (2013).
16. N. Cezard, S. L. Mehaute, J. L. Gouët, M. Valla, D. Goular, D. Fleury, C. Planchat, and A. Dolfi-Bouteyre, "Performance assessment of a coherent DIAL-Doppler fiber lidar at 1645 nm for remote sensing of methane and wind," Opt. Express, OE **28**, 22345–22357 (2020).
17. J. Caron, Y. Durand, J.-L. Bezy, and R. Meynart, "Performance modeling for A-SCOPE: a space-borne lidar measuring atmospheric CO2," in *Lidar Technologies, Techniques, and Measurements for Atmospheric Remote Sensing V* (International Society for Optics and Photonics, 2009), Vol. 7479, p. 74790E.
18. N. Menyuk and D. K. Killinger, "Temporal correlation measurements of pulsed dual CO2 lidar returns," Opt. Lett., OL **6**, 301–303 (1981).
19. T. Ehrenreich, R. Leveille, I. Majid, K. Tankala, G. Rines, and P. Moulton, "1-kW, all-glass Tm: fiber laser," presented at SPIE Photonics West 2010: LASE Fiber Lasers VII: Technology, Systems, and Applications (January 28, 2010).
20. A. Kobyakov, M. Sauer, and D. Chowdhury, "Stimulated Brillouin scattering in optical fibers," Adv. Opt. Photon., AOP **2**, 1–59 (2010).
21. L. Li, B. Zhang, K. Yin, L. Yang, and J. Hou, "1 mJ nanosecond all-fiber thulium-doped fiber laser at 2.05 μm," Opt. Express, OE **23**, 18098–18105 (2015).
22. E. Lucas, L. Lombard, Y. Jaouën, S. Bordais, and G. Canat, "1 kW peak power, 110 ns single-frequency thulium doped fiber amplifier at 2050 nm," Appl. Opt., AO **53**, 4413–4419 (2014).
23. J.-P. Cariou, B. Augere, and M. Valla, "Laser source requirements for coherent lidars based on fiber technology," Comptes Rendus Physique **7**, 213–223 (2006).
24. C. B. Layne, W. H. Lowdermilk, and M. J. Weber, "Multiphonon relaxation of rare-earth ions in oxide glasses," Phys. Rev. B **16**, 10–20 (1977).
25. J. H. Churnside and H. T. Yura, "Speckle statistics of atmospherically backscattered laser light," Appl. Opt., AO **22**, 2559–2565 (1983).
26. L. M. Frantz and J. S. Nodvik, "Theory of Pulse Propagation in a Laser Amplifier," Journal of Applied Physics **34**, 2346–2349 (1963).
27. S. Ryu, S. Yamamoto, H. Taga, N. Edagawa, Y. Yoshida, and H. Wakabayashi, "Long-haul coherent optical fiber communication systems using optical amplifiers," Journal of Lightwave Technology **9**, 251–260 (1991).
28. G. A. Wagner and D. F. Plusquellic, "Multi-frequency differential absorption LIDAR system for remote sensing of CO2 and H2O near 1.6 μm," Opt. Express, OE **26**, 19420–19434 (2018).

29. K. Numata, J. R. Chen, S. T. Wu, J. B. Abshire, and M. A. Krainak, "Frequency stabilization of distributed-feedback laser diodes at 1572 nm for lidar measurements of atmospheric carbon dioxide," Appl. Opt., AO **50**, 1047–1056 (2011).
30. E. A. Curtis, T. Bradley, G. P. Barwood, C. S. Edwards, N. V. Wheeler, R. Phelan, D. J. Richardson, M. N. Petrovich, and P. Gill, "Laser frequency stabilization and spectroscopy at 2051 nm using a compact CO2-filled Kagome hollow core fiber gas-cell system," Opt. Express, OE **26**, 28621–28633 (2018).
31. R. M. Measures, *Laser Remote Sensing: Fundamentals and Applications* (Krieger Pub. Co, 1992).